

Deuteron- ^3He scattering using nucleon- ^3He optical potentials fitted to four-body amplitudes

A. Deltuva, D. Jurčiukonis

Institute of Theoretical Physics and Astronomy, Vilnius University, Saulėtekio al. 3, LT-10257 Vilnius, Lithuania

Abstract

Deuteron- ^3He reactions in the 15 to 40 MeV range are studied using a three-body model where the constructed nonlocal optical potentials rely on rigorous nucleon- ^3He scattering calculations. The differential cross section for the elastic scattering and neutron transfer reaction is predicted quite well up to 90 deg scattering angles. The importance of the Pauli term in complex potentials is demonstrated.

Key words: Few-body reactions, Faddeev-Yakubovsky equations, nonlocal optical potential, Pauli repulsion

1. Introduction

Introduction of optical potentials into the nuclear reaction theory enabled the reduction of a many-nucleon problem, encountered in the nucleon-nucleus scattering, to an effective two-body problem. The enormous complexity of the many-body problem in the continuum for a long time restricted the construction of optical potentials to the phenomenological approach, where model parameters were adjusted to the experimental data, such as in the Chappel Hill [1], Koning and Delaroche [2], Weppner et al. [3] and many other optical potentials. Many-nucleon structure calculations using various methods such as the microscopic mean field, the no-core shell model, Green's function Monte Carlo, coupled cluster approach, self-consistent Green's function progressed significantly in the last decades, opening the doors for approximate extensions to the continuum and microscopic calculations of the optical potentials as reviewed in Ref. [4]. For example, quite a typical approach is folding the microscopically calculated nuclear densities with the nucleon-nucleon interaction [5–7], either bare or G -matrix one. A prerequisite for this approach, limited to the first order scattering term, is high enough beam energy. This way some methods, like those based on the mean-field description, were able to develop microscopic optical potentials also for heavy nuclei above mass number $A = 200$. In contrast, the lightest nuclei such

as ^3H and ^3He remain beyond the reach of those methods as the individual character of their constituent nucleons plays an important role, and it is not even clear to what extent the optical potential description can be successful. Since nucleon- ^4He scattering calculations are available only below the breakup threshold [8–10], we study the lighter isotope ^3He , with rigorous nucleon- ^3He scattering calculations available at energies well above the breakup threshold [11,12]. Furthermore, ^3He has the nucleon separation energy around 5 MeV, which is quite a typical excitation energy for many light nuclei, in contrast to exceptionally tightly bound ^4He , and thus might be more suitable to draw conclusions. Therefore we aim to construct the optical models for proton (p) and neutron (n) interactions with ^3He based on rigorous continuum calculations, a unique feature among the optical potentials. Beside the quality in reproducing the experimental nucleon-nucleus scattering data, the further criterion is the ability to describe more complicated reactions such as the deuteron-nucleus scattering. Thus, another goal of the present work is the application of the developed nucleon- ^3He potentials to the deuteron- ^3He elastic scattering, breakup, and the neutron transfer reaction $^3\text{He}(d,p)^4\text{He}$ at energies well above the breakup threshold of the involved nuclei. As the transfer reaction at very low energy is of high importance for the termonuclear fusion, in the regime below the breakup threshold it has also been studied using the no-core shell model with continuum [13,14].

A somehow similar idea has been explored in the past for ^5H resonance study in the three-body $^3\text{H} + n + n$ model by

Email addresses: arnoldas.deltuva@tfai.vu.lt (A. Deltuva), darius.jurciukonis@tfai.vu.lt (D. Jurčiukonis).

developing effective neutron- ^3H potential [15]. It contained several local Gaussian terms whose parameters were fitted to phase shifts below the inelastic threshold. Consequently, the imaginary part was vanishing. An important feature of that potential was a strong partial-wave dependence of its parameters, quite common in few-nucleon systems. In the present work we aim to develop complex potentials valid over a broader energy range with open inelastic channels, but we also expect the need for strongly partial-wave dependent parameters.

Section 2 recalls microscopic four-nucleon reaction calculations, section 3 describes and validates the developed nucleon- ^3He optical potentials, while section 4 reminds the three-cluster deuteron- ^3He scattering equations. Sections 5 and 6 contain the deuteron- ^3He scattering results and our conclusions, respectively.

2. Four-body calculation of the nucleon- ^3He scattering

A rigorous quantum-mechanical description for the nucleon scattering from the three-nucleon bound state can be given by the Alt, Grassberger and Sandhas (AGS) equations [16] for transition operators $\mathcal{U}_{\beta\alpha}$ that constitute a momentum-space integral equation formulation of the Faddeev-Yakubovsky (FY) four-particle theory [17]. Previous benchmark calculations [18,19] with alternative theoretical frameworks, namely, the hyperspherical harmonics expansion method [20,21] and the coordinate-space FY equations [22,23], performed below the breakup threshold, revealed good agreement between the three methods, confirming their reliability. The symmetrized form of the AGS equations [24], most convenient for the four-nucleon system in the isospin formalism, reads

$$\mathcal{U}_{11} = -(G_0 t G_0)^{-1} P_{34} - P_{34} U_1 G_0 t G_0 \mathcal{U}_{11} + U_2 G_0 t G_0 \mathcal{U}_{21}, \quad (1a)$$

$$\mathcal{U}_{21} = (G_0 t G_0)^{-1} (1 - P_{34}) + (1 - P_{34}) U_1 G_0 t G_0 \mathcal{U}_{11}, \quad (1b)$$

where G_0 is the free resolvent that gives rise to energy-dependence of the transition operators, $t = v + vG_0t$ is the two-nucleon transition operator derived from the two-nucleon potential v including the screened Coulomb force for the two-proton pair, and

$$U_\alpha = P_\alpha G_0^{-1} + P_\alpha t G_0 U_\alpha \quad (2)$$

are subsystem transition operators. The subscripts 1 and 2 label the (12,3)4 and (12)(34) partitions, while P_α and P_{34} are permutation operators, explained in Ref. [24] together with other details. The on-shell elements of \mathcal{U}_{11} between the neutron- ^3He or proton- ^3He channel states yield the respective amplitudes for the elastic scattering.

The AGS equations (1) are solved in the momentum-space partial-wave representation where they become a large system of up to 30000 equations in three continuous variables, the Jakobi momenta. Two special procedures

are employed: (i) screening and renormalization method [25–28] to include the Coulomb interaction between the protons, and (ii) the complex-energy method with special weights [29] to deal with integrable but highly complicated singularities in the integral equation kernel; see Refs.[11,12,29] for more details and example results for scattering observables.

3. Nucleon- ^3He optical potential

Typically, the parameters of phenomenological optical potentials are determined by fitting the experimental data for rather few selected scattering observables, such as the differential cross section, analyzing power and inelastic cross sections. As we base our nucleon- ^3He optical potential on rigorous microscopic calculations, the quantities to be reproduced are the theoretical elastic scattering amplitudes. Furthermore, since the transition operators contain full information on the physical system including inelastic processes, reproducing elastic amplitudes implies also reproducing the predictions for the inelastic cross section, that can be calculated via optical theorem from the imaginary part of the forward scattering amplitude. In the neutron- ^3He case it has contributions not only from the breakup but also from the charge exchange $^3\text{He}(n, p)^3\text{H}$ and proton transfer $^3\text{He}(n, d)^2\text{H}$ reactions. One might perhaps question whether those channels can be accounted for by the optical potential, since the proton- ^3H threshold is even lower in energy than the neutron- ^3He one. However, this is relevant near the threshold only, while in the considered energy regime the elastic neutron- ^3He cross section exceeds the ones for charge exchange and proton transfer by one order of magnitude [12].

Previous studies [11,12] found that the experimental data for nucleon- ^3He scattering in the 10 to 35 MeV regime are best reproduced using the inside-nonlocal outside-Yukawa (INOY04) two-nucleon potential by Doleschall [30,22]. Thus, the scattering amplitudes obtained solving four-nucleon AGS equations with this potential will be used as input for the construction of nucleon- ^3He optical potentials.

We demand that solutions of the two-body Lippman-Schwinger equation

$$T_N = V_N + V_N G_0 T_N \quad (3)$$

with the nucleon- ^3He optical potentials V_N reproduce accurately the respective microscopic elastic scattering amplitudes over the energy range of roughly 13 to 30 MeV, which is relevant for the application to the deuteron- ^3He scattering and where the four-body calculations are available. There is some arbitrariness in choosing the form of the potential. Optical potentials in general are energy-dependent, however, it is well known that the energy dependence is weaker if the potential is nonlocal in the coordinate space. Using the proton- ^{24}Mg elastic and inelastic scattering as example [31] we demonstrated recently that an energy-independent nonlocal optical potential may provide a rea-

sonable description of the experimental data in finite energy range. For this reason we assume the nonlocal form also for the nucleon- ^3He optical potential, i.e.,

$$V_N(\mathbf{r}', \mathbf{r}) = \frac{1}{2} [H(|\mathbf{r}' - \mathbf{r}|)V(r) + V(r')H(|\mathbf{r}' - \mathbf{r}|)], \quad (4)$$

where \mathbf{r}' and \mathbf{r} are final and initial distances between particles, and

$$H(x) = \pi^{-3/2} \rho^{-3} e^{-(x/\rho)^2} \quad (5)$$

is the nonlocality function with the nonlocality range ρ . As in Ref. [31] we use typical value $\rho = 1$ fm. The local part we represent by several Gaussian terms as it is quite common for effective potentials [7,15], i.e.,

$$V(r) = \sum_{j=1}^2 V_j e^{-(r/R_j)^2} + iW_c e^{-(r/R_w)^2} + [V_s e^{-(r/R_s)^2} + iW_s e^{-(r/R_w)^2}] (\delta_s \mathbf{s}_N \cdot \mathbf{L} + \delta_t \hat{S}_{12}) \quad (6)$$

where V_k and W_k are strengths of various real and imaginary terms, R_k are their Gaussian radii, and \mathbf{s}_N , \mathbf{L} and \hat{S}_{12} are the nucleon spin, nucleon- ^3He orbital angular momentum and tensor [32] operators, respectively. Additionally, δ_s and δ_t being either 1 or 0 control the presence/absence of spin-orbit and tensor terms. The proton- ^3He potential is supplemented by the Coulomb force, which below the Coulomb radius of 1.7 fm is taken as the potential of uniformly charged sphere. First fitting attempt using single parameter set for all partial waves was not successful, consistently with previous neutron- ^3H studies [15], and confirming our expectation for a need of partial-wave dependent parameters. We therefore fitted each partial wave separately. In doing this we tried to keep as few fitting parameters as possible. That is, in many cases some terms in Eq. (6) could be set to zero, or at least share the same radius. Furthermore, we found that the tensor term $\delta_t = 1$ is only important for coupled partial waves with $L = J \pm 1$, $S = 1$, while the spin-orbit term $\delta_s = 1$ is only important for coupled partial waves with $L = J$, $S = 0, 1$, where J and S is the total angular momentum and spin, respectively. Thus, tensor and spin orbit terms are not included simultaneously, and are missing in the uncoupled waves. We also found that in the regime up to 30 MeV the partial waves with $L > 3$ can be safely neglected. In order to estimate uncertainties, we developed several parameter sets for optical potentials. Quite typically, they differ in range and strength, i.e., smaller radii imply larger strengths. While some changes can be seen in small components of two-body scattering amplitudes on a fine scale, we verified that the predictions for the nucleon- ^3He and deuteron- ^3He scattering observables are not visibly affected.

Except for the 1S_0 neutron- ^3He partial wave all the other nucleon- ^3He $L = 0$ waves are Pauli repulsive. This is reflected by mostly positive V_j values in those waves. Another way [33] to take into account this Pauli repulsion is to use attractive potential supplemented by a strong repulsive nonlocal term $|b\rangle\Gamma\langle b|$. This approach is often used in simple

nuclear structure models for the nucleon-nucleus real binding potential to project out the state $|b\rangle$ corresponding to an occupied shell. An example close to our present study is the real low-energy nucleon- ^4He potential in the $L = 0$ state [34]. While the differences in the two approaches for three-body bound state calculations are moderate at most, in scattering calculations they become tremendous [34,35]. To the best of our knowledge, such a Pauli-repulsive term has not yet been included into complex optical potentials, and will be investigated in the present work. The S -wave component of the deuteron and ^3He overlap $\langle dq(L=0)|^3\text{He}\rangle = \langle q|b\rangle$, q being the spectator nucleon momentum, is an appropriate representation of the occupied $L = 0$ state in ^3He . For simplicity we add the same term $|b\rangle\Gamma\langle b|$ to the potential (4) in the 3S_1 wave and, for proton- ^3He , in the 1S_0 wave, and refit the parameters of (6). The strength of the Pauli-repulsive term is set to $\Gamma = 1$ GeV, but we verified that results become largely independent of Γ once it exceeds few hundred MeV.

Furthermore, a modification of the neutron- ^3He potential in the 1S_0 partial wave is needed for the calculation of the $^3\text{He}(d, p)^4\text{He}$ reaction. The potential must be real to simulate the ^4He nucleus as the bound state of ^3He and neutron, though due to its large binding energy of about 20.6 MeV this is not a good model. We demand the effective neutron- ^3He potential to reproduce not only this binding energy, but also that the bound-state wave function mimics (up to a factor) the $\langle ^3\text{He}|^4\text{He}\rangle$ overlap function, ensuring that the spatial and momentum distribution of the neutron in our model is similar to that in the ^4He nucleus. To estimate the uncertainties, we used two choices for this binding potential (6), namely, $V_1 = -2V_2 = -132.848$ MeV and $V_1 = -V_2 = -156.113$ MeV, with radii $R_1 = 2R_2 = 1.7$ fm in both cases. Such approach of approximating the single-particle wave function by an overlap becomes quite common in including the many-body nuclear structure information into the few-body description of nuclear reactions [36]. In Faddeev or AGS few-body calculations the bound-state wave function must be normalized to unity, thus, the calculated single-particle theoretical cross section has to be multiplied by the corresponding norm of the overlap, i.e., the spectroscopic factor (SF), as explained in detail in Ref. [36]. The SF from our microscopic ^3He and ^4He calculations with INOY04 potential equals to 1.65. A similar approach in representing the overlaps by solutions of the single-particle Schrödinger equation was developed in Ref. [37]. Despite using different nuclear Hamiltonian, the resulting overlap and $\text{SF} \approx 1.6$ turn out to be close to ours. The agreement becomes even better in a recent update [38] using soft nuclear forces, leading to $\text{SF} = 1.65$.

We demonstrate the quality of our optical potentials by comparing with results of microscopic four-body calculations. As examples in Figs. 1 and 2 we show the proton- ^3He and neutron- ^3He differential cross sections, achieving quite a satisfactory agreement between the predictions of two- and four-body models. The agreement is almost perfect around the middle of the considered energy region, but

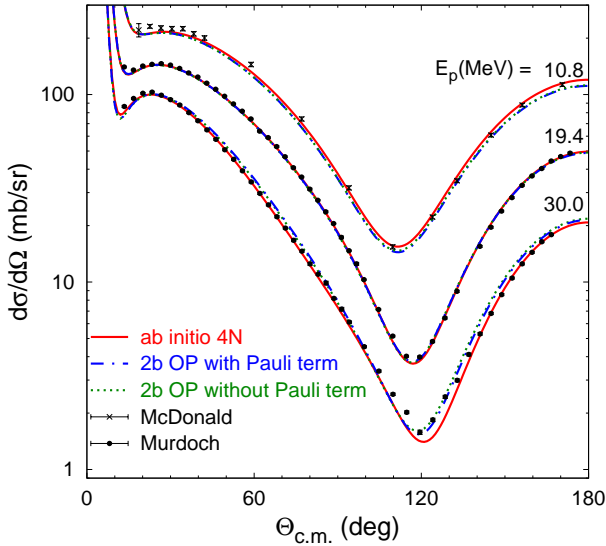


Fig. 1. Differential cross section for the proton- ^3He elastic scattering at 10.8, 19.4 and 30 MeV beam energy as function of the c.m. scattering angle. Results of microscopic four-nucleon calculations (solid curves) are compared with predictions obtained using two-body optical potentials (2b OP), either without (dotted curves) or with (dashed-dotted curves) the Pauli term. The experimental data are from Refs. [39,40].

some deviations occur at lowest and highest energies. However, even those deviations are smaller than the spread of the four-nucleon calculations obtained with different realistic two-nucleon potentials [11,12]. The only more sizable deviation occurs near the neutron- ^3He differential cross section minimum at higher energy when using a real potential in the 1S_0 partial wave supporting the ^4He bound state and thereby not fitted to the scattering amplitudes. A further evidence of the accuracy can be found in the Supplemental material, together with the parameters of the developed optical potentials.

4. Three-body AGS equations

Deuteron scattering from a nucleus A has been calculated in many works using the Faddeev or its equivalent AGS transition operator formalism, see Ref. [35] for the deuteron- ^4He example. The three-body transition operators are obtained from the AGS equation

$$U_{ba} = \bar{\delta}_{ba} G_0^{-1} + \sum_{m=p,n,A} \bar{\delta}_{bm} T_m G_0 U_{ma}, \quad (7)$$

where the usual odd-man-out notation is used, $\bar{\delta}_{ba} = 1 - \delta_{ba}$, the nucleon-nucleus transition operators T_p and T_n are given by Eq. (3), and T_A by an analogous equation with the neutron-proton potential. For consistency we take the INOY04, though we verified that using other realistic potentials yields very similar results. The solution of the scattering equations (7) is again performed using the momentum-space partial-wave representation, while more

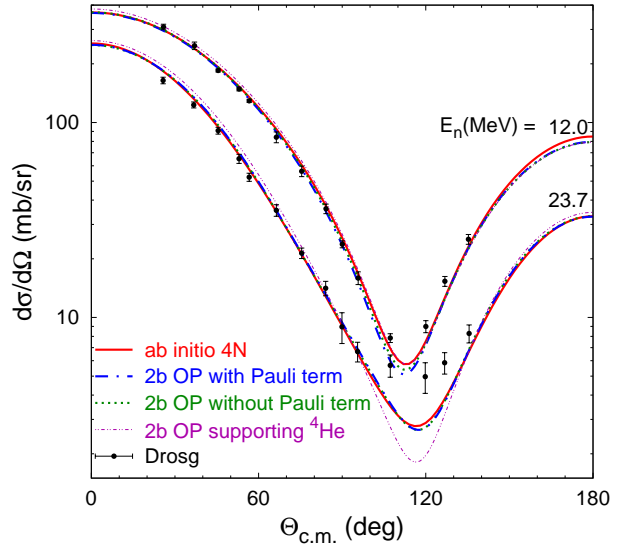


Fig. 2. Differential cross section for the neutron- ^3He elastic scattering at 12 and 23.7 MeV beam energy. Curves as in Fig. 1, while additional dashed-double-dotted curves label results with a real neutron- ^3He potential in the 1S_0 partial wave supporting the ^4He bound state. The experimental data are from Ref. [41].

technical details can be found in Refs. [35,31] and references therein.

On-shell matrix elements of U_{ba} taken between the two- or three-cluster channel states determine the physical transition amplitudes for the respective reactions [35], from where the differential cross sections are calculated, as for example outlined in Ref. [12].

5. Results

Using the nonlocal interaction models described in Sec. 3 we solve the AGS equations (7) and calculate deuteron- ^3He differential cross sections at deuteron beam energy $E_d = 14.6, 19.7, 24.9, 30.0, 34.9$ and 39.9 MeV, where the experimental data from Berkeley laboratory [42] are available. In Fig. 3 we compare experimental data for elastic differential cross sections with three calculations, that isolate two dynamics ingredients: (i) including or excluding the Pauli term, and (ii) including or excluding the ^4He bound state by using real or complex neutron- ^3He potential in the 1S_0 partial wave. The latter effect of the bound state turns out to be very small, discernible only near the minimum at large scattering angles, with no any visible sensitivity to the parametrization of the binding potential. In contrast, the effect of the Pauli term is very large, significantly changing the shape of the angular distribution. Though none of the predictions are in a perfect agreement with data, those including the Pauli term are considerably closer to the data, especially in the shape at intermediate and backward angles. One may perhaps argue that $E_d = 14.6$ MeV is too low for our optical potentials fitted from 13 to 30 MeV nucleon energy, as typically one takes energy-dependent nucleon optical potentials at $E_d/2$. This might explain a abit larger

discrepancy at small angles. On the other hand, one can question also the experimental data which does not show monotonic variation in energy, for example, the 30 MeV data at forward angles lies between the 19.7 and 24.9 MeV data. In contrast, our theoretical predictions vary smoothly with energy.

In Fig. 4 we compare experimental data for the transfer reaction ${}^3\text{He}(d, p){}^4\text{He}$ to several theoretical predictions including or excluding the Pauli term. Again, the effect of this term turns out to be sizable, especially at larger scattering angles, where the shape of the angular distribution is changed dramatically, leading to one more local maximum of the differential cross section. Although the absolute value is significantly underpredicted in this region, this change of shape due to the Pauli term is clearly supported by the experimental data. The comparison of results with different neutron- ${}^3\text{He}$ binding potentials in the 1S_0 partial wave reveals some sensitivity, but is far less important than the Pauli term.

Finally, in Fig. 5 we show that the Pauli term affects significantly also the differential cross section in the deuteron breakup reaction. In the case of fully exclusive breakup the observables are often shown for fixed solid scattering angles Ω_a (polar θ_a and azimuthal ϕ_a) of two detected particles as functions of the arclength S in the plane of their kinetic energies [35]. In Fig. 5 those two particles are assumed to be ${}^3\text{He}$ and proton.

6. Conclusions

We considered elastic, transfer and breakup reactions in deuteron collisions with ${}^3\text{He}$ nuclei. We have not solved the underlying five-nucleon problem rigorously, but our study does not rely on the experimental information beyond the one contained in the realistic two-nucleon potential INOY04. We used exact solutions of four-nucleon AGS scattering equations for the transitions operators and, as an intermediate step, developed nucleon- ${}^3\text{He}$ optical potentials quite accurately reproducing scattering amplitudes from four-body calculations. We constructed also a model containing the Pauli term, not included up to now into complex optical potentials. Inserting those potentials into three-body AGS equations, that treat the ${}^3\text{He}$ nucleus as an inert particle but exactly account for the breakup of the deuteron, led to predictions for deuteron- ${}^3\text{He}$ reactions.

In cases of the elastic scattering and ${}^3\text{He}(d, p){}^4\text{He}$ reaction the comparison with the experimental differential cross section revealed quite a good agreement up to about 90 deg scattering angles, but discrepancies remained at larger angles.

The model including the Pauli term is considerably closer to the data, especially in the shape at intermediate and backward angles. Noteworthy, our description of the ${}^3\text{He}(d, p){}^4\text{He}$ transfer reaction is considerably more successful than the DWBA analysis of Ref. [42], though it used initial- and final-channel optical potentials well fitted

to the elastic deuteron- ${}^3\text{He}$ and proton- ${}^4\text{He}$ data.

We speculate that the large-angle discrepancy, especially in the deuteron elastic scattering, is a signature for the reaction mechanism specific to very light nuclei but not included in our model. Namely, the reaction can proceed via the one-proton exchange, i.e., the ${}^3\text{He}(d, {}^3\text{He})d$ reaction, where the deuteron picks one proton from ${}^3\text{He}$ becoming a "new" ${}^3\text{He}$, while the target ${}^3\text{He}$ after losing one proton becomes a "new" deuteron. Qualitatively the same reaction mechanism is present in the nucleon-deuteron scattering, where it is responsible for the backward angle cross section increase. In four-nucleon reactions it is a two-nucleon transfer that produces a similar effect.

Our finding of general importance for nuclear reaction description is the significance of the Pauli term not only for real but also for complex optical potentials. Further studies have to be performed to evaluate the relevance of the Pauli term in heavier systems.

Authors thank P. U. Sauer for discussions during his stay at Vilnius University. This work has received funding from the Research Council of Lithuania (LMTLT) under Contract No. S-MIP-22-72. Part of the computations were performed using the infrastructure of the Lithuanian Particle Physics Consortium.

References

- [1] R. L. Varner, W. J. Thompson, T. L. McAbee, E. J. Ludwig, T. B. Clegg, Phys. Rep. 201 (1991) 57.
- [2] A. J. Koning, J. P. Delaroche, Nucl. Phys. A713 (2003) 231.
- [3] S. P. Weppner, R. B. Penney, G. W. Diffendale, G. Vittorini, Phys. Rev. C 80 (2009) 034608.
- [4] C. Hebborn, *et al.*, Journal of Physics G: Nuclear and Particle Physics 50 (2023) 060501.
- [5] M. Gennari, M. Vorabbi, A. Calci, P. Navrátil, Phys. Rev. C 97 (2018) 034619.
- [6] M. Vorabbi, M. Gennari, P. Finelli, C. Giusti, P. Navrátil, R. Machleidt, Phys. Rev. C 105 (2022) 014621.
- [7] T. Furumoto, K. Tsubakihara, S. Ebata, W. Horiuchi, Phys. Rev. C 99 (2019) 034605.
- [8] K. M. Nolle, S. C. Pieper, R. B. Wiringa, J. Carlson, G. M. Hale, Phys. Rev. Lett. 99 (2007) 022502.
- [9] S. Quaglioni, P. Navrátil, Phys. Rev. Lett. 101 (2008) 092501.
- [10] R. Lazauskas, Phys. Rev. C 97 (2018) 044002.
- [11] A. Deltuva, A. C. Fonseca, Phys. Rev. C 87 (2013) 054002.
- [12] A. Deltuva, A. C. Fonseca, Phys. Rev. C. 90 (2014) 044002.
- [13] P. Navrátil, S. Quaglioni, Phys. Rev. Lett. 108 (2012) 042503.
- [14] G. Hupin, S. Quaglioni, P. Navrátil, Nature Communications 10 (2019) 351.
- [15] R. de Diego, E. Garrido, D. Fedorov, A. Jensen, Nuclear Physics A 786 (2007) 71.
- [16] P. Grassberger, W. Sandhas, Nucl. Phys. B2 (1967) 181; E. O. Alt, P. Grassberger, and W. Sandhas, JINR report No. E4-6688 (1972).
- [17] O. A. Yakubovsky, Yad. Fiz. 5 (1967) 1312 [Sov. J. Nucl. Phys. 5, 937 (1967)].
- [18] M. Viviani, A. Deltuva, R. Lazauskas, J. Carbonell, A. C. Fonseca, A. Kievsky, L. E. Marcucci, S. Rosati, Phys. Rev. C 84 (2011) 054010.
- [19] M. Viviani, A. Deltuva, R. Lazauskas, A. C. Fonseca, A. Kievsky, L. E. Marcucci, Phys. Rev. C 95 (2017) 034003.

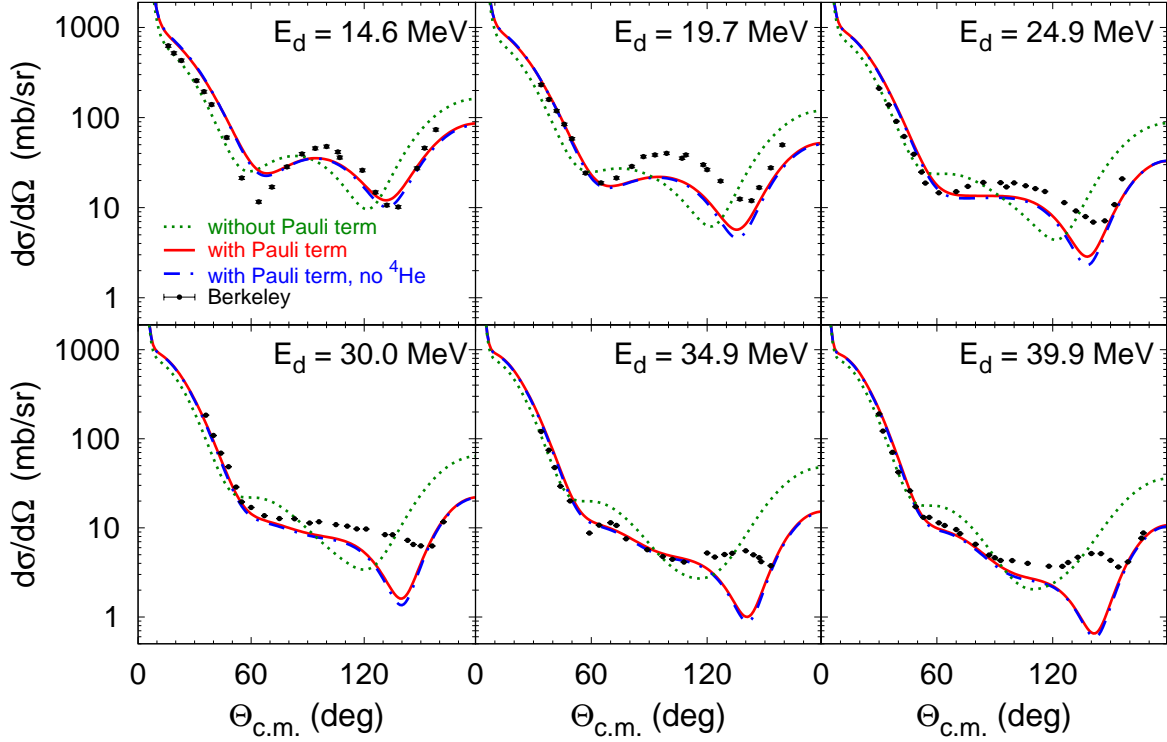


Fig. 3. Differential cross section for deuteron- ^3He elastic scattering in the energy range 14.6 to 39.9 MeV. Predictions using optical potentials with/without Pauli term and with/without bound neutron- ^3He state are compared with the experimental data from Ref. [42].

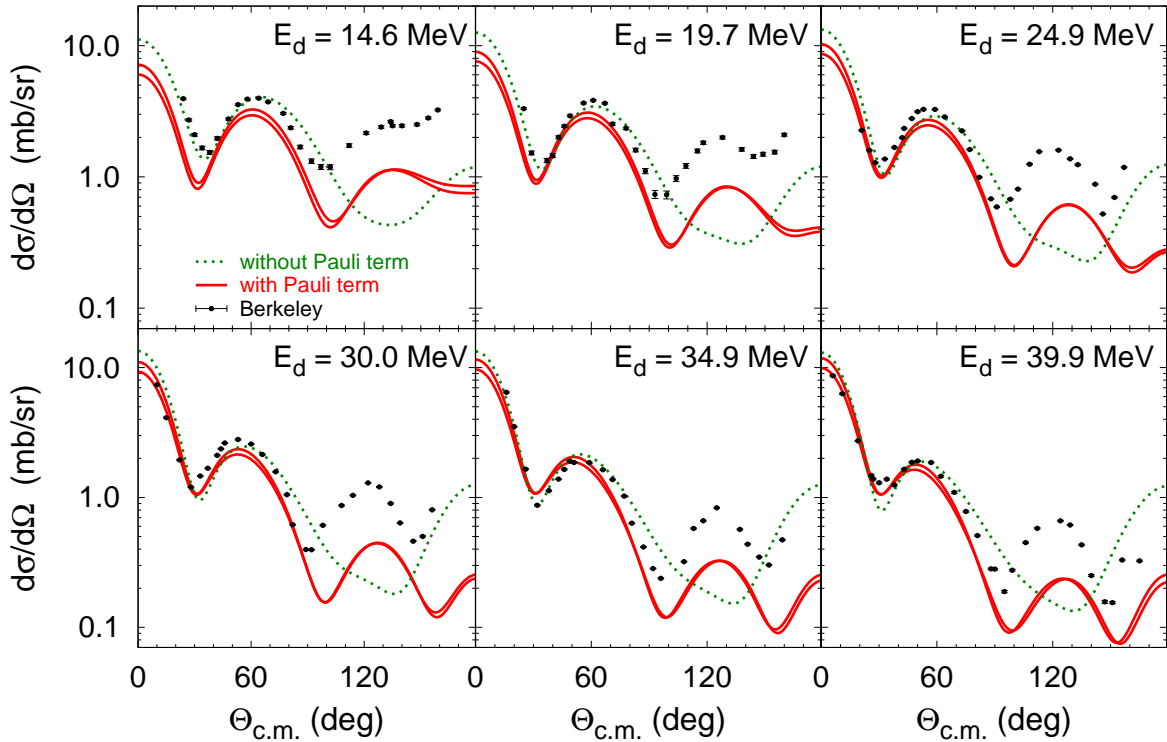


Fig. 4. Differential cross section for the $^3\text{He}(d, p)^4\text{He}$ reaction in the energy range 14.6 to 39.9 MeV. Predictions using optical potentials with/without Pauli term are compared with the experimental data from Ref. [42]. The two solid curves correspond to different neutron- ^3He binding potentials in the 1S_0 partial wave.

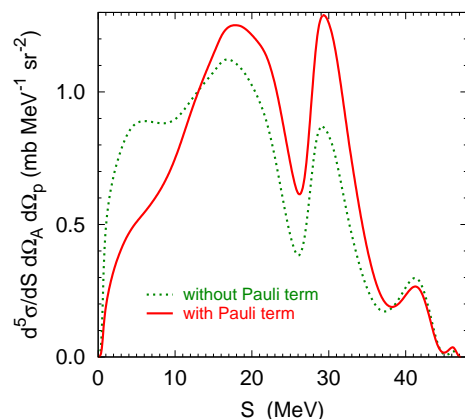


Fig. 5. Fivefold differential cross section for the deuteron breakup in collision with ${}^3\text{He}$ at 30 MeV beam energy as function of the arclength S . The final state kinematical configuration is characterized by ${}^3\text{He}$ and proton scattering angles $(\theta_A, \phi_A) = (15^\circ, 0^\circ)$ and $(\theta_p, \phi_p) = (45^\circ, 180^\circ)$. Predictions of optical potentials with and without Pauli term are compared. The ${}^4\text{He}$ bound state is not supported.

- [20] M. Viviani, A. Kievsky, S. Rosati, E. A. George, L. D. Knutson, Phys. Rev. Lett. 86 (2001) 3739.
- [21] A. Kievsky, S. Rosati, M. Viviani, L. E. Marcucci, L. Girlanda, J. Phys. G 35 (2008) 063101.
- [22] R. Lazauskas, J. Carbonell, Phys. Rev. C 70 (2004) 044002.
- [23] R. Lazauskas, Phys. Rev. C 79 (2009) 054007.
- [24] A. Deltuva, A. C. Fonseca, Phys. Rev. C 75 (2007) 014005.
- [25] J. R. Taylor, Nuovo Cimento B 23 (1974) 313.
- [26] M. D. Semon, J. R. Taylor, Nuovo Cimento A 26 (1975) 48.
- [27] E. O. Alt, W. Sandhas, Phys. Rev. C 21 (1980) 1733.
- [28] A. Deltuva, A. C. Fonseca, P. U. Sauer, Phys. Rev. C 71 (2005) 054005.
- [29] A. Deltuva, A. C. Fonseca, Phys. Rev. C 86 (2012) 011001(R).
- [30] P. Doleschall, Phys. Rev. C 69 (2004) 054001.
- [31] A. Deltuva, D. Jurčiukonis, Phys. Rev. C 107 (2023) 064602.
- [32] V. G. J. Stoks, R. A. M. Klomp, C. P. F. Terheggen, J. J. de Swart, Phys. Rev. C 49 (1994) 2950.
- [33] V. Kukulin, V. Krasnopol'sky, V. Voronchev, P. Sazonov, Nuclear Physics A 417 (1984) 128.
- [34] I. J. Thompson, B. V. Danilin, V. D. Efros, J. S. Vaagen, J. M. Bang, M. V. Zhukov, Phys. Rev. C 61 (2000) 024318.
- [35] A. Deltuva, Phys. Rev. C 74 (2006) 064001.
- [36] A. Deltuva, E. Cravo, R. Crespo, D. Jurčiukonis, Physics Letters B 855 (2024) 138859.
- [37] I. Brida, S. C. Pieper, R. B. Wiringa, Phys. Rev. C 84 (2011) 024319.
- [38] R.B. Wiringa,
<https://www.phy.anl.gov/theory/research/overlaps/>.
- [39] D. G. McDonald, W. Haeberli, L. W. Morrow, Phys. Rev. 133 (1964) B1178.
- [40] B. T. Murdoch, D. K. Hasell, A. M. Sourkes, W. T. H. van Oers, P. J. T. Verheijen, R. E. Brown, Phys. Rev. C 29 (1984) 2001.
- [41] M. Drogg, D. K. McDaniels, J. C. Hopkins, J. D. Seagrave, R. H. Sherman, E. C. Kerr, Phys. Rev. C 9 (1974) 179.
- [42] R. Roy, F. Seiler, H. E. Conzett, F. N. Rad, Phys. Rev. C 24 (1981) 2421.

Supplemental material for "Deuteron- ^3He scattering using nucleon- ^3He optical potentials fitted to four-body amplitudes"

A. Deltuva, D. Jurčiukonis

Institute of Theoretical Physics and Astronomy, Vilnius University, Saulėtekio al. 3, LT-10257 Vilnius, Lithuania

1. Parameters of nucleon- ^3He optical potentials

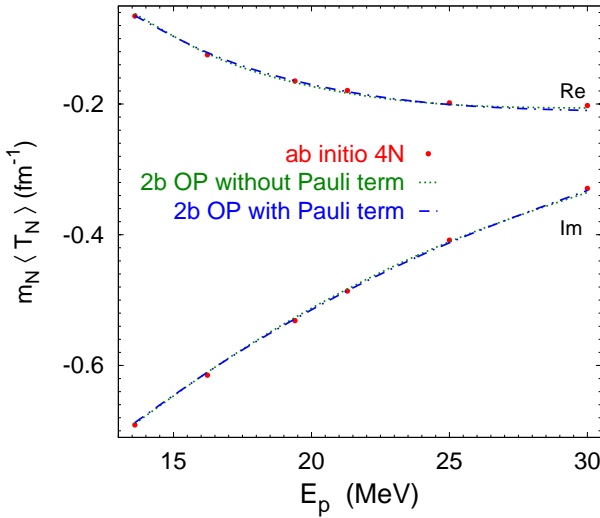


Fig. 1. Real and imaginary parts of the proton- ^3He elastic scattering amplitude (after separating the point Coulomb contribution) in the 1S_0 partial wave as functions of the beam energy. Results of microscopic four-nucleon calculations (points) are compared with predictions obtained using two-body optical potentials (2b OP), either without (dotted curves) or with (dashed-dotted curves) the Pauli term.

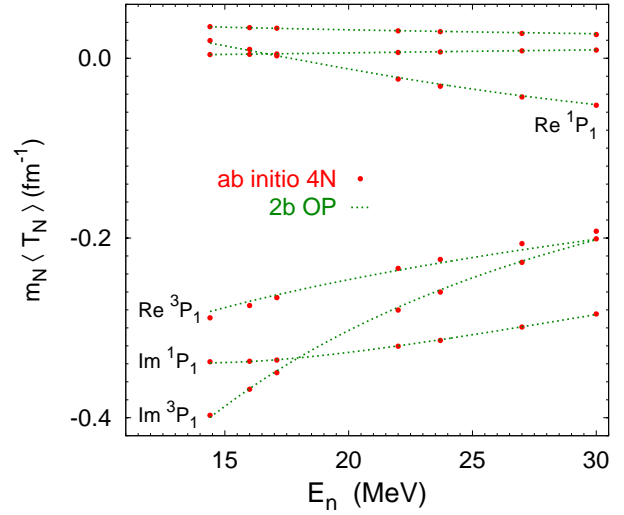


Fig. 2. Real and imaginary parts of the neutron- ^3He elastic scattering amplitudes in the coupled $^1P_1 - ^3P_1$ partial wave as functions of the beam energy. Results of microscopic four-nucleon calculations (points) are compared with predictions obtained using two-body optical potentials (dotted curves). The diagonal amplitudes are labelled, the non-diagonal ones are located near the zero line.

Table 1

Parameters of the proton- ^3He optical potential. Strengths are in units of MeV, while radii are in units of fm. The parameters for spin-orbit or tensor forces are identical in both coupled waves, and are listed just once.

$^{2S+1}L_J$	V_1	R_1	V_2	R_2	W_c	R_w	V_s	R_s	W_s
1S_0	82.032	2.186	9.031	3.977	-2.193	2.075			
3P_0	-46.343	1.840	-4.510	3.347	-1.917	1.679			
3S_1	100.000	2.022	5.202	4.277	-7.000	1.850	1.813	2.653	-1.105
3D_1	-70.000	1.344	2.328	3.919	-21.000	1.850			
1P_1	-19.957	2.116	-3.841	3.841	-9.517	1.125	39.364	1.332	-1.000
3P_1	-14.354	2.116	-9.416	3.841	-8.426	1.125			
3P_2	-95.729	1.613	-6.754	3.391	-2.589	1.297	-5.735	2.411	0.865
3F_2			-5.184	3.391	-5.741	2.714			
1D_2	-16.981	2.367	4.304	3.902	-5.000	2.004	10.000	1.782	-0.763
3D_2	-20.000	2.367	2.731	3.902	-10.024	2.004			
3D_3	-60.000	1.875	2.563	3.872	-5.000	2.228			
1F_3			-1.239	4.206	-5.000	2.247	20.000	1.221	-0.143
3F_3	-100.000	1.624	-2.361	4.206	-10.000	2.247			
3F_4	-60.000	1.720	-2.219	4.000	-10.000	2.400			

Table 2

Parameters of the neutron- ^3He optical potential.

$^{2S+1}L_J$	V_1	R_1	V_2	R_2	W_c	R_w	V_s	R_s	W_s
1S_0	-71.053	2.730	12.757	4.947	-12.327	4.982			
3P_0	-91.075	2.093	7.782	4.997	-28.208	1.285			
3S_1	70.784	2.023	18.484	2.926	-14.145	1.746	2.872	2.563	-1.969
3D_1	-26.868	2.266	10.362	2.994	-27.676	1.746			
1P_1	-136.992	1.453			-30.000	2.282	39.134	1.221	-3.211
3P_1	-24.326	1.231	-12.228	4.000	-5.088	2.282			
3P_2	-150.000	1.188	-10.978	5.000	-4.037	1.298	-2.010	1.700	10.000
3F_2			-2.690	3.872	-10.107	2.807			
1D_2	150.000	1.036	-19.166	3.109	-28.077	2.629	150.000	0.934	-1.437
3D_2	-149.999	1.390	6.930	3.104	-6.672	2.629			
3D_3	-50.000	2.106	6.045	3.380	-12.000	1.876			
1F_3	-55.155	2.079	1.562	3.530	-3.095	2.533	17.898	1.394	-0.372
3F_3	-20.922	1.039	-1.252	4.261	-18.444	2.533			
3F_4	-48.346	1.584	-2.967	3.852	-11.244	2.730			

Table 3

Parameters of the proton- ^3He optical potential in the presence of the Pauli term.

$^{2S+1}L_J$	V_1	R_1	V_2	R_2	W_c	R_w	V_s	R_s	W_s
1S_0			-17.639	3.544	-4.732	0.700			
3S_1	-96.946	1.165	-4.142	3.691	-0.768	2.344	4.929	2.617	-0.919
3D_1			3.980	3.691	-8.060	2.344			

Table 4

Parameters of the neutron- ^3He optical potential in the presence of the Pauli term.

$^{2S+1}L_J$	V_1	R_1	V_2	R_2	W_c	R_w	V_s	R_s	W_s
3S_1	-4.022	1.830	-35.936	2.715	-3.017	1.733	6.516	2.686	1.552
3D_1	-64.913	1.830	21.735	2.715	-19.226	1.733			